



# Development and *in vitro* characterization of rifapentine microsphere-loaded bone implants: a sustained drug delivery system

Zhen Wang<sup>1</sup>, Xinghua Song<sup>1,2</sup>, Huan Yang<sup>3</sup>, Abulikemu Maimaitiaili<sup>1</sup>, Tengfei Wang<sup>1</sup>

<sup>1</sup>Department of Orthopaedics, The First Affiliated Hospital of Xinjiang Medical University, Urumqi 830011, China; <sup>2</sup>Department of Orthopaedics, The First Affiliated Hospital of Jinan University, Guangzhou 510630, China; <sup>3</sup>The Linfen Center for Disease Control and Prevention, Linfen 041000, China

**Contributions:** (I) Conception and design: Z Wang, X Song; (II) Administrative support: X Song; (III) Provision of study materials or patients: Z Wang, X Song; (IV) Collection and assembly of data: Z Wang, X Song, H Yang, A Maimaitiaili, T Wang; (V) Data analysis and interpretation: Z Wang, X Song; (VI) Manuscript writing: All authors; (VII) Final approval of manuscript: All authors.

**Correspondence to:** Xinghua Song. Department of Orthopaedics, The First Affiliated Hospital of Xinjiang Medical University, No 393 New Medical Road, Urumqi 830011, China. Email: songxinghua19@163.com.

**Background:** This study aimed to develop and evaluate a sustained drug delivery system for the treatment of osteoarticular tuberculosis (TB) to address the issues surrounding low drug concentration in lesions and bone defects or nonunion after debridement.

**Methods:** The effects of rifapentine on the proliferation and cell cycle of bone marrow mesenchymal stem cells (BMSCs) were evaluated by Cell Counting Kit-8 (CCK-8) and flow cytometry. Rifapentine polylactic acid (PLA) sustained-release microspheres (RPSMs) were prepared through the double emulsion solvent evaporation method and investigated the antibacterial activity *in vitro*. In this study, two sustained drug delivery systems were prepared by integrating RPSMs and BMSCs into hydroxyapatite/ $\beta$ -tricalcium phosphate (HA/ $\beta$ -TCP) or allogeneic bone. We evaluated these drug delivery systems for dynamics of drug release and osteogenic ability by *in vitro* release test, alkaline phosphatase (ALP) and alizarin red staining, and real-time PCR.

**Results:** The results showed that rifapentine concentrations up to 45.0  $\mu$ g/mL had no effect on cell proliferation and cell cycle. The encapsulation and drug loading efficiency of the fabricated RPSMs were 78.11% $\pm$ 1.16% and 35.57% $\pm$ 0.85%, respectively. The RPSMs had uniform particle size distribution and a long-term anti-bacterium effect. The HA/ $\beta$ -TCP-implanted drug delivery system was found to be more effective in reducing the burst release and having a longer duration of sustained release and retention compared to allogeneic bone. The ALP and alizarin red staining and real-time PCR results showed that it had excellent osteoconductive and osteoinductive properties.

**Conclusions:** In conclusion, the sustained drug delivery system with HA/ $\beta$ -TCP as scaffold material represents a potential new strategy for TB infections and bone defects.

**Keywords:** Rifapentine; bone marrow mesenchymal stem cells (BMSCs); sustained-release microsphere; hydroxyapatite/ $\beta$ -tricalcium phosphate (HA/ $\beta$ -TCP); allogeneic bone; drug-loaded composite scaffold

Submitted Jan 01, 2020. Accepted for publication Jan 20, 2020.

doi: 10.21037/apm.2020.03.13

View this article at: <http://dx.doi.org/10.21037/apm.2020.03.13>

## Introduction

Tuberculosis (TB), which is caused by *Mycobacterium TB*, is a chronic consuming disease and one of the leading causes of death around the world (1). Accounting for approximately 1–3% (2) of total TB cases and 35% of extrapulmonary TB cases (3), osteoarticular TB is the most common form of extrapulmonary TB (4). Frequently accompanied by a degree of structural damage and deformity, osteoarticular TB impacts the stability and function of the bones and joints (5), often leading to surgical treatment.

Although surgical and medical treatments for osteoarticular TB have seen improvements in recent years, the removal of the bacteria still proves difficult. Therefore, apart from the debridement operation, following surgical treatment, recurrence can only be prevented by long-term medication (6,7). However, due to the ineffective concentration of anti-TB drugs at infected sites, long-term medication, adverse side effects, and bone defects or nonunion after debridement, curing osteoarticular TB is challenging (8,9). Combining drug treatments with bone tissue repair appears to offer a feasible approach to overcoming this problem and improving the therapeutic effect. Herein, we developed novel anti-TB drug delivery systems, which simultaneously achieved a longer duration of sustained release and retention and had much better effects in promoting bone formation.

A member of the rifamycin group, rifapentine is a semisynthetic antibiotic and has been approved to be one of the first-line anti-TB drugs by the US Food and Drug Administration (FDA) (10). In comparison with rifampicin, rifapentine has an antibacterial spectrum similar to that of rifampin, exhibits greater antibacterial effect and stronger penetrating ability (11), and has a longer drug elimination half-life and fewer adverse reactions. Polylactic acid (PLA) is a non-toxic, bioresorbable polymer with good biocompatibility, safety, and biodegradability (12). It has been approved by the US and European FDA as a drug delivery carrier material for controlled drug release (13). For these reasons, rifapentine and PLA were chosen as the drug and carrier to formulate rifapentine polylactic acid sustained-release microspheres (RPSMs).

Bone defects are common among individuals with osteoarticular TB, and bone graft materials are needed to fill these bone defects and ensure a tight junction between the implant and the host bone. The materials commonly used in bone grafts are autologous, allogeneic, or synthetic. Although the transplantation of autologous bone remains the “gold standard” in bone repair technology, it is

also associated with limited availability and high donor morbidity (14,15). Therefore, both allografts and synthetic grafts are considered as suitable alternatives for bone regeneration.

Due to being easily accessible and having multipotent differentiation ability, bone marrow mesenchymal stem cells (BMSCs) have been applied extensively for bone tissue engineering (16,17). In the treatment of bones and joints, BMSCs have been applied in the clinical field of osteonecrosis treatment to repair of bone defects (18). Therefore, we used BMSCs as they are regarded as one of the most promising kinds of osteogenic stem cells for promoting bone formation.

In this study, RPSMs and BMSCs were combined with hydroxyapatite/ $\beta$ -tricalcium phosphate (HA/ $\beta$ -TCP) composite material or allogenic bone to develop drug delivery systems. These two drug delivery systems were evaluated for dynamics of drug release and osteogenic induction ability through *in vitro* experiments, providing a fresh approach to the clinical treatment of osteoarticular TB.

## Methods

### Materials

PLA (MV =30,000, Shandong Medical Devices Co. Ltd., Jinan, China), Rifapentine (Sichuan Mingxin Pharmaceutical Co. Ltd., Chengdu, China), gelatin, chloroform, methanol, ultra-pure water, and p-nitrophenol (Sigma-Aldrich, St Louis, MO, USA), Dulbecco's modified Eagle's medium (DMEM) (Hyclone, Logan, UT, USA), fetal bovine serum (Gibco BRL, Grand Island, NY, USA), propidium iodide (BD Biosciences, San Jose, CA, USA), osteogenic, adipogenic and chondrogenic induction medium (Cyagen Biosciences Co. Ltd., Suzhou, China), modified Lowenstein-Jensen medium culture (Ouke Biosciences Co. Ltd., Wuhu, China), Cell Counting Kit-8 (Dojindo, Kumamoto, Japan), synthetic HA/ $\beta$ -TCP scaffold (composed of 60% HA and 40%  $\beta$ -TCP, Bi-Ostetic, Berkeley, CA, USA), BCIP/NBT chromogenic kit, Alizarin Red dye solution, Oil Red O stain kit and Alcian Blue Cartilage Stain solution were purchased from Solarbio Co., Ltd (Beijing, China). Anti-CD14, anti-CD44, and anti-CD45 antibodies were purchased from Thermo Fisher Scientific (Waltham, MA, USA), anti-CD29 antibodies were purchased from Merck Millipore (Billerica, MA, USA), and anti-Collagen I, anti-Osteocalcin and anti-GAPDH antibodies were purchased from Abcam (Cambridge, UK). *Mycobacterium TB* was

provided by Xinjiang Academy of Animal Science.

### ***Cell isolation, culture, and identification***

Rabbit BMSCs were harvested from 12-week-old New Zealand white rabbits. The rabbits were sacrificed under anesthesia, and their bilateral femurs and tibias were removed under sterile conditions and placed in PBS. The metaphyses were cut off on a sterile platform, before approximately 5 mL of marrow was flushed out with 10 mL of DMEM. Primary cells were cultured in DMEM supplemented with fetal bovine serum (10%, w/v), penicillin (100 units/mL), and streptomycin (100 µg/mL). The cells were resuspended at 5 million per 100 mm<sup>2</sup> dish and incubated at 37 °C with 5% of CO<sub>2</sub> under a humidified atmosphere of 95% air. After incubation lasting 5 days, the culture medium was changed to remove non-adherent cells. After 14 days of primary culture, the cells were isolated and serially subcultured for further experiments.

The cell surface antigens of CD29, CD44, CD45, and CD14 in the third passage BMSCs were detected by flow cytometry. The digested BMSCs were suspended at a cell density of 5×10<sup>5</sup> cells/mL and labeled with antibodies against CD29 (1:100 dilution), CD44 (1:100 dilution), CD45 (1:100 dilution), and CD14 (1:100 dilution) for 1 hour at 4 °C. The cells were subsequently washed with PBS three times before incubation with the secondary antibodies (dilution, 1:2,000, Thermo Fisher Scientific) for 2 hours in a black chamber at 4 °C. The cells were washed with PBS and fixed in 4% paraformaldehyde. Flow cytometry was performed on an FACSCalibur cytometer (BD Biosciences, San Jose, CA, USA) using CellQuest software (BD Biosciences).

To assess the multilineage differentiation potential of BMSCs, osteogenic, adipogenic, and chondrogenic differentiation were induced. BMSCs were seeded onto 6-well plates at 2×10<sup>4</sup> cells/cm<sup>2</sup> and incubated in osteogenic, adipogenic, and chondrogenic induction mediums, respectively. The medium was changed twice a week. After differentiating for 14 days, the BMSCs were stained with Alizarin red solution, Oil Red O solution, and Alcian blue solution, according to the manufacturer's instructions.

### ***CCK-8 assay for cell survival in vitro***

The evaluation of the general survival of cells *in vitro* was carried out with CCK-8 in line with the manufacturer's instructions. The rabbit BMSCs were divided into five groups, which were incubated in a 96-well plate at 5×10<sup>3</sup>

cells/mL, with 3 wells per group. The cells were cultured in medium containing 5 different concentrations of rifapentine (15.0, 30.0, 45.0, 60.0, and 75.0 µg/mL). Absorbance was measured using a microplate spectrophotometer (Multiskan MK3, Thermo Fisher Scientific, Waltham, MA, USA) at a wavelength of 450 nm. The CCK-8 colorimetric method was used to assess cell proliferation daily.

### ***Flow cytometry for cell cycle analysis***

Three generations of rabbit BMSCs were cultured in medium with or without rifapentine. After incubation lasting 6 days, the cells were harvested and then centrifuged at 800 ×g for 5 minutes and washed twice with PBS. Subsequently, the cells were fixed in cold 75% ethanol for 5 h, then washed twice with PBS and incubated with 0.5 mL of PBS containing 100 µg/mL RNase and 50 µg/mL propidium iodide at 37 °C for 30 min away from light. Cell cycle distribution was analyzed by measuring DNA content with a flow cytometer (BD Biosciences).

### ***Microsphere preparation***

Since rifapentine is a hydrophobic compound, RPSMs were prepared using the double emulsion–solvent evaporation method. Briefly, 100 mg of PLA was accurately weighed and dissolved in 5 mL of dichloromethane (DCM), and 100 mg of rifapentine was dissolved into the polymer solution. The polymer-solvent-drug solution was cooled to 4 °C, then placed on an ice block and treated with an ultrasonic cell pulverizer for 1.5 min to achieve emulsification. After stirring at high speed at 1,500 rpm, the emulsion was injected into 25 mL of 0.5% gelatin aqueous solution through a micro-injection pump, emulsified for 5 min, and then stirred gently for 5–7 hours to ensure it was evenly mixed. After continuous stirring for a period of time, DCM became completely volatilized with the microspheres solidified. The microspheres obtained in the suspension were suction-filtered through a 0.88 µm pore size filtration membrane, collected, washed with distilled water, and centrifuged three times at 800 ×g. Finally, the collected microspheres were freeze-dried for 24 h and stored in a refrigerator at –20 °C.

### ***High performance liquid chromatography (HPLC) and standard curves***

HPLC was used to determine the concentration of

rifapentine in the samples. The HPLC system (Shimadzu, Kyoto, Japan) includes the Shimadzu LC-10ATVP pump, Shimadzu SPD-10AVP UV-vis detector, and LC-solution software package (Shimadzu). The size of the Shim-pack VP-ODS chromatographic column was 150 mm × 4.6 mm, 5 µm; flow speed was 1.0 mL/minute; detection wavelength was 336 nm; column temperature was 25 °C; sample size was 10 µL; mobile phase A was methanol; mobile phase B was ultra-pure water; and the sample was eluted by gradient elution. P-nitrophenol was used as an internal standard. The standard curves with concentrations ranging from 0.25 to 32 µg/mL ( $R^2 = 0.999$ ) were drawn by measuring the contents of rifapentine standards.

### *Physicochemical properties of RPSMs*

Measurements of particle size and size distribution of the microspheres were taken using particle size analyzer (Mastersizer 3000, Malvern Instruments Ltd., Malvern, UK). The mean volume diameter measured was taken as the mean particle size of the microspheres. To detect the encapsulation and drug loading efficiency of the RPSMs, 5 mg of RPSMs was accurately weighed in a 10 mL flask and DCM (0.1 mL) was added to break down the microsphere structure. This was followed by calibrating and dissolving the microspheres by adding an appropriate amount of methanol. After filtration through a millipore membrane filter, the rifapentine content was measured using HPLC, the encapsulation and drug loading efficacy of the prepared microspheres were measured three times, and the average encapsulation and drug loading efficiency of the microspheres were calculated. The encapsulation efficiency was defined as the percent ratio of actual drug loading to theoretical drug loading, while the drug loading efficiency was defined as the percent ratio of the actual drug content to the total microsphere weight. The morphology of RPSMs was observed under fluorescence microscope (Leica DM6000B, Wetzlar, Germany) and scanning electron microscope (SEM, JSM-6510LV, JEOL, Tokyo, Japan).

### *In vitro antibacterial activity*

In this study, Mycobacterium TB H37Rv (ATCC 27294) was used to investigate the antibacterial performance of RPSMs *in vitro*, and the suspension of mycobacterium TB was diluted to about  $1 \times 10^6$  cfu/mL for standby. The agar diffusion test with a filter paper was used to determine the susceptibility of Mycobacterium TB to RPSMs. About

10 mg of RPSMs was suspended in 10 mL of sterile PBS for 6 hours, before the 6 mm diameter sterile filter paper was immersed in it. After 30 minutes, the filter papers were withdrawn, and the excess liquid was drained off. About 100 µL of bacterial suspensions were homogeneously spread on modified Lowenstein-Jensen medium culture, and the filter paper was carefully placed in the center of the medium. The culture was carried out for 4 and 8 weeks in an incubator with a CO<sub>2</sub> concentration of 5.0% and a temperature of 37 °C to observe whether an inhibition zone was present. Rifapentine and non-loaded drug filter paper were used as positive and negative controls.

### *The preparation of sustained drug delivery systems and in vitro release test*

Cancellous bone grafts (allogenic bone) were processed from the vertebral locations of rabbits (3 mm in diameter and length). Briefly, after fat and connective tissue had been removed, the grafts were rinsed with sterile water at 37 °C for 30 min. They were then incubated in a mixture of chloroform and methanol v/v, 1/1 under constant agitation for a 2-hour period. After this, the grafts were sonicated 3 times in methanol for 15 min to remove chloroform and were washed twice with sterile deionized water to remove the methanol. Consequently, the grafts were freeze-dried, sterilized by epoxyethane gas and kept at room temperature for later use.

The drug delivery systems were constructed taking into account the different graft materials. In brief, the BMSCs were suspended in osteogenic induction medium at a cell density of  $3 \times 10^6$  cells/mL. Then, 3 mg of the RPSMs was mixed with 300 µL of osteogenic induction medium and added dropwise to the scaffold (HA/β-TCP or allogenic bone) to form two drug delivery systems: system A (IBMSCs + RPSMs + HA/β-TCP) and system B (IBMSCs + RPSMs + allograft), respectively. The system was transferred to a petri dish after 5 h in culture, and 5 mL of osteogenic induction medium was added. The medium was changed and collected every other day. Following incubation for 14 days, the cells were washed twice with PBS, fixed with 4% paraformaldehyde overnight, dehydrated gradually by ethanol, and sprayed with gold. The adhesion and growth of cells in the scaffold were observed using SEM.

The collected medium was centrifuged twice at 800 ×g, and the supernatant was collected, and its drug content was measured using HPLC. The rifapentine release curve and cumulative percentage release curve of rifapentine were calculated and plotted.

### *Evaluating the effects of the drug delivery systems on osteogenic differentiation of cells*

The cells were divided into 5 groups, with 400  $\mu$ L of BMSC suspension in each group. The groups were as follows: group A (BMSCs): cells were cultured in normal medium; group B (induced BMSCs, IBMSCs): cells were cultured in osteogenic induction medium; group C (IBMSCs + RPSMs): cells were mixed with 3 mg of RPSMs and cultured in osteogenic induction medium; groups D and E (IBMSCs + RPSMs + HA/ $\beta$ -TCP, IBMSCs + RPSMs + allograft): cells were mixed with 3 mg of RPSMs and added dropwise to HA/ $\beta$ -TCP or allogenic bone, respectively, and cultured in osteogenic induction medium. The cells were digested with trypsin after 7 and 14 days of culture, before being counted and plated again at  $1 \times 10^5$ /well, cultured in an incubator for 3 days, and subjected to alkaline phosphatase (ALP) and Alizarin Red staining according to the manufacturer's instructions.

### *Quantitative RT-PCR analysis of mRNA expression*

On days 14 and 21, quantitative real-time polymerase chain reaction (PCR) was performed to investigate the expression of collagen I and osteocalcin on days 14 and 21. Total RNA was isolated using TRIZOL reagent (Invitrogen, Thermo Fisher Scientific, Waltham, MA, USA) according to the manufacturer's instructions. Total RNA was reverse transcribed and amplified using a RevertAid First Strand cDNA Synthesis Kit (Thermo Fisher Scientific). Quantitative real-time PCR assays were performed using the DyNAmo Flash SYBR Green qPCR kit (Thermo Fisher Scientific). GAPDH was used as the internal control. The primer sequences were as follows: collagen I (Rabbit): forward primer (5'-CCCAGAAACAGACGACAAACAAC-3'), reverse primer (5'-AACGGCAAAAACAAATCTCCAAA-3'); osteocalcin (Rabbit): forward primer (5'-GCCCTCACTCTTGTCGCCCTGCT-3'), reverse primer (5'-ACCACCTCGCTGCCCTCCCTCTT-3'); GAPDH (Rabbit): forward primer (5'-ACCTGACCTGCCGCCTGGAGAAAGC-3'), reverse primer (5'-GGAGACGACCTGGTCCTCGGTGTAG-3').

### *Statistical analysis*

Each measurement represents mean  $\pm$  standard deviation (SD) of three independent experiments or an experiment of triplicate assay. All data were analyzed using the SPSS

22.0 software (IBM Corporation, Armonk, NY, USA). The one-way analysis of variance (ANOVA) with Tukey's post hoc test was employed to make comparisons between the groups. Differences were considered significant at  $P < 0.05$ .

## **Results**

### *Characterization of BMSCs*

Identification of the morphology, purity, and differentiation of the third passage BMSCs was performed. As *Figure 1A* reveals, BMSCs were uniform spindle-shaped with clones distributed as radial clusters when viewed under a light microscope (BX53, Olympus, Tokyo, Japan). The positive rates of CD29, CD44, CD45, and CD14, which were detected by flow cytometry, were 95.90%, 93.90%, 1.33%, and 1.82%, respectively (*Figure 1B*), indicating the high purity of third passage BMSCs. Under standard *in vitro* differentiating conditions, BMSCs had a good ability for osteogenic, adipogenic, and chondrogenic differentiation, as is seen in *Figure 1C*.

### *The effect of rifapentine on cell proliferation and cycle*

The cell survival rate of BMSCs in the presence of 45.0  $\mu$ g/mL rifapentine was consistent with those of normal cells (*Figure 2A*). Cell cycle analysis revealed that in comparison with the drug-free cells (*Figure 2B*), there was no significant change in the proportion of cells at each phase of cells in the presence of 45.0  $\mu$ g/mL rifapentine (*Figure 2C*).

### *Physicochemical properties of microspheres*

The RPSMs were red in color, powdery, and non-adhesive. The RPSMs were spherical in shape with a smooth surface, and there were small pores on the surface of individual microspheres under the SEM (*Figure 3A*). The mean particle size of the RPSMs was  $27.67 \pm 2.05$   $\mu$ m, with symmetrical distribution (*Figure 3B*). The encapsulation and drug loading efficiency of the RPSMs were  $78.11\% \pm 1.16\%$  and  $35.57\% \pm 0.85\%$ , respectively.

### *In vitro antibacterial activity*

At 4 weeks, the bacterial inhibition assays showed that the maximum inhibition zone diameters of the RPSMs and rifapentine in the medium containing Mycobacterium TB were  $18.67 \pm 2.52$  mm and  $19.67 \pm 1.53$  mm, respectively, with

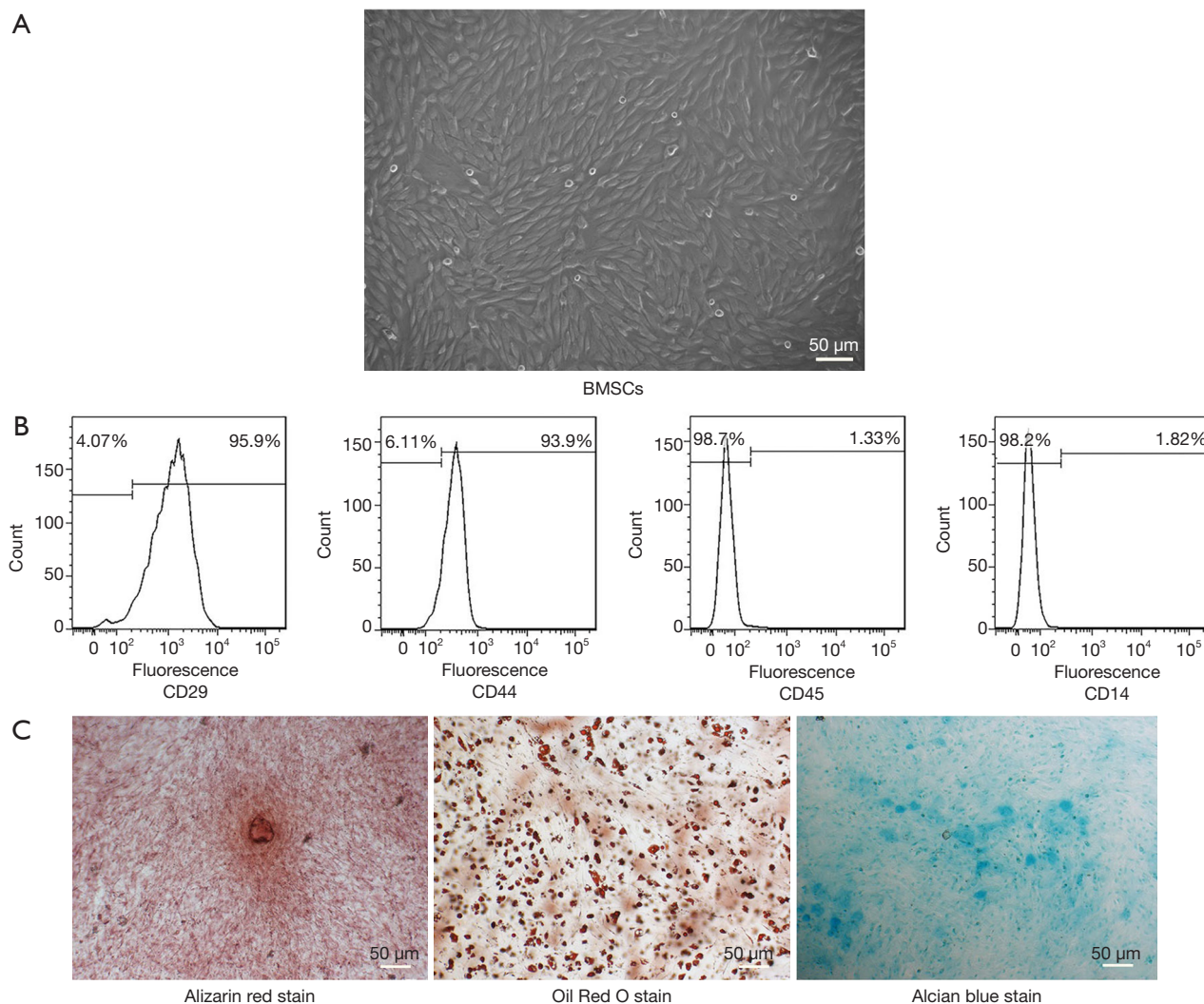


**Figure 1** Morphology and features of BMSCs. (A) The spindle-shaped morphology of BMSCs is seen in passage 3 (original magnification: 100 $\times$ , scale bar =50  $\mu$ m). (B) The isolated BMSCs were characterized by a flow cytometer. BMSCs were positive for CD29 and CD44 but negative for CD45 and CD14. (C) Osteogenic, adipogenic, and chondrogenic differentiation of BMSCs and staining with Alizarin red, Oil Red O, and Alcian blue, respectively (original magnification: 100 $\times$ , scale bar =50  $\mu$ m). BMSCs, bone marrow mesenchymal stem cells.

no significant difference ( $P>0.05$ ). At 8 weeks, the maximum inhibitory zone diameter of RPSMs was  $18.33\pm 2.08$  mm and that of rifapentine was  $13.33\pm 1.53$  mm. Significant difference was observed between the two groups ( $P<0.05$ ) (Figure 4).

#### *The preparation and drug release curve of the drug delivery system*

The structure of HA/ $\beta$ -TCP and allogenic bone was observed by SEM (Figure 5A,B). The ultrastructural imaging of the two systems by SEM showed the RPSMs and BMSCs to be tightly adhered to the scaffold surface. The

cells grew well and had a spindle-shaped morphology, with cellular pseudopods extending around the microspheres (Figure 5C,D).

The HPLC was used to calculate the drug concentration, and the rifapentine release curve and cumulative percentage release curve of rifapentine were plotted (Figure 6A,B). The two systems formed by HA/ $\beta$ -TCP and allogenic bone in our tests exhibited similar biphasic release profiles. During the burst release phase, a large amount of rifapentine was released from the two systems within 6 and 8 days, with drug release peaks of 19.08 and 30.82  $\mu$ g/mL, respectively, followed by a period of smooth decreased release rate for

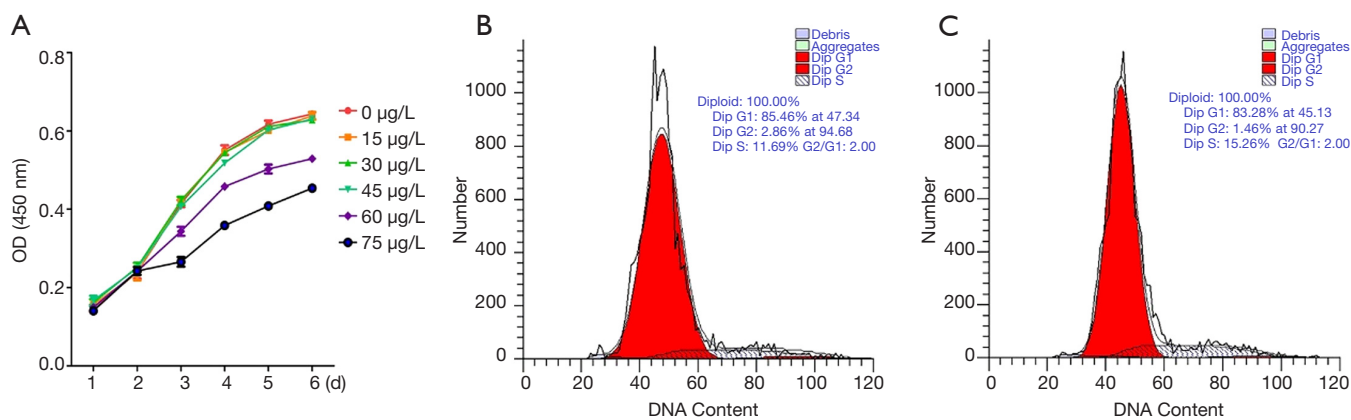


**Figure 2** The effect of rifapentine on cell proliferation and cycle. (A) The proliferation curve of BMSCs. (B) Cell cycle detection results of drug-free cells. (C) Cell cycle detection results of drug-treated cells. BMSCs, bone marrow mesenchymal stem cells.

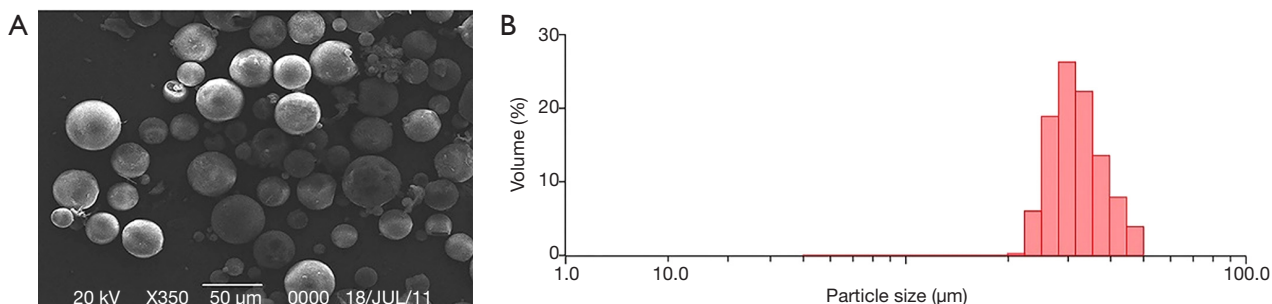


**Figure 3** Morphology and features of RPSMs. (A) Scanning electron micrograph of prepared RPSMs (300 $\times$  magnification, scale bar = 50  $\mu$ m). (B) Particle size distribution of RPSMs. RPSMs, Rifapentine Poly(lactic Acid) Sustained-Release Microspheres.

nearly 60 days. At the end of the *in vitro* release tests, the cumulative release amount of rifapentine in the two systems reached 90.24% $\pm$ 0.22% (HA/ $\beta$ -TCP) and 83.90% $\pm$ 1.00% (allogenic bone), respectively.

#### Evaluation of the effects of drug delivery system on osteogenic differentiation of cells

With the purpose of evaluating the effects of the two drug delivery systems on differentiation of BMSCs, BMSCs were cultured for 7 and 14 days and then stained with ALP and alizarin red (Figure 7). At 7 days, ALP staining was found to be negative in group A and positive in the other four groups, with results demonstrating the BMSCs had differentiated into osteoblasts. Groups D and E both demonstrated significantly stronger ALP staining intensity when compared to groups B and C. The same trend was observed for alizarin red staining at 14 days, with the number of calcium nodules increasing significantly in

groups D and E.

In each group of cells, quantitative real-time PCR was used to analyze the mRNA expression levels of osteoblast differentiation markers (Figure 8). The results showed that the collagen I and osteocalcin mRNA levels in groups D and E were significantly increased at 7 and 14 days when compared to groups B and C. Furthermore, the expressions of collagen I and osteocalcin were not significantly different between groups D and E, nor between groups B and C.

#### Discussion

The clinical treatment of osteoarticular TB is extremely challenging and results in ischemia and necrosis of the bone and abscess formation in the infective sites. The disability rate among patients whose spine joints are affected is high, due to structural damage and deformity as well as spinal cord or nerve function damage (19,20), which often lead to surgical treatment and long-term medication. Effective

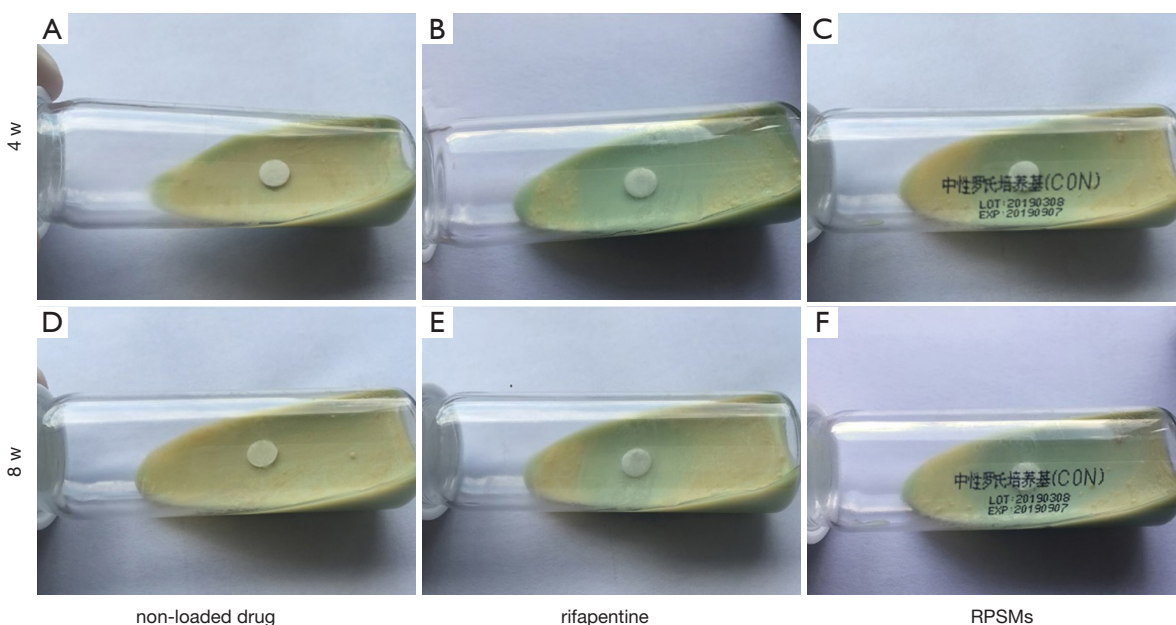


**Figure 4** *In vitro* antibacterial activity. (A) and (D), (B) and (E), and (C) and (F) show the bacterial inhibiting areas of non-loaded drug filter paper, rifapentine, and RPSMs, respectively, at weeks 4 and 8. RPSMs, Rifapentine Poly(lactic acid) Sustained-Release Microspheres.

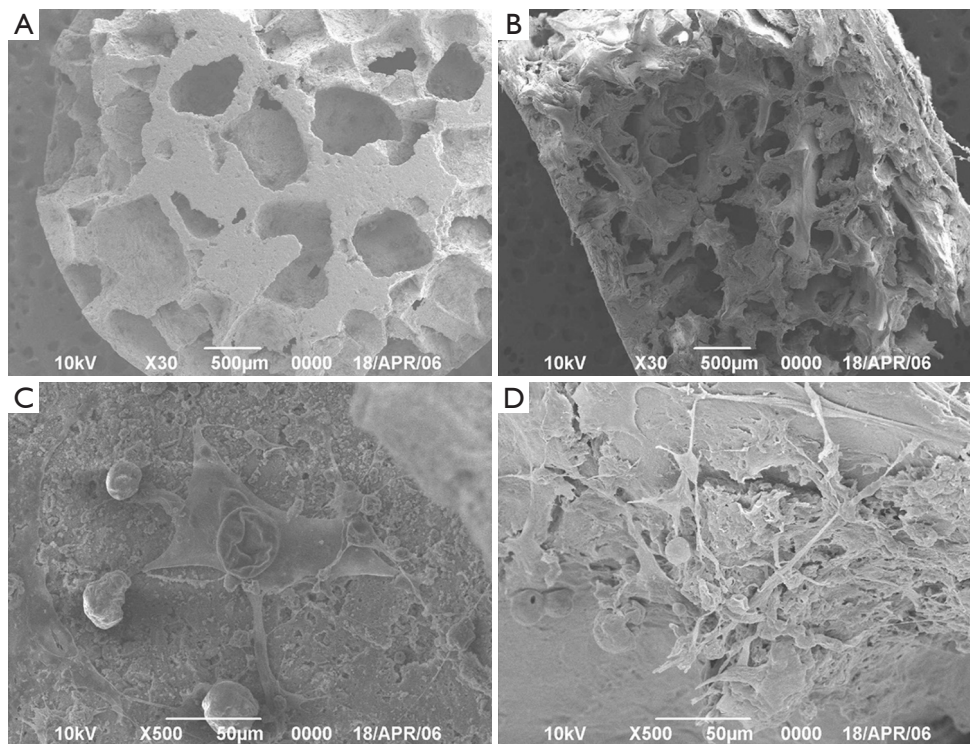


**Figure 5** Scanning electron micrograph of scaffolds and systems. (A) HA/β-TCP (30× magnification, scale bar =500 μm). (B) Allogenic bone (30× magnification, scale bar =500 μm); (C) System A, IBMSCs + RPSMs + HA/β-TCP (300× magnification, scale bar =50 μm). (D) System B, IBMSCs + RPSMs + allograft (300× magnification, scale bar =50 μm). BMSCs, bone marrow mesenchymal stem cells; RPSMs, Rifapentine Poly(lactic acid) Sustained-Release Microspheres.

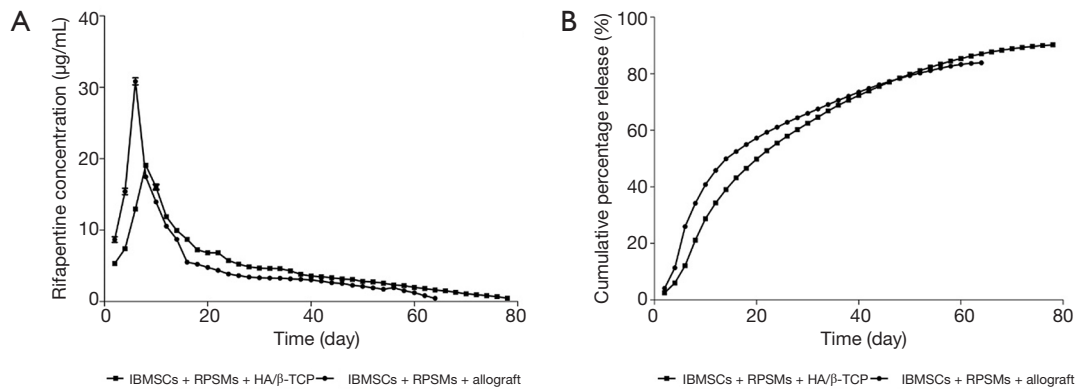


**Figure 6** *In vitro* release test results. (A) *In vitro* rifapentine release curve of systems A (IBMSCs + RPSMs + HA/β-TCP) and B (IBMSCs + RPSMs + allograft); (B) the *in vitro* cumulative percentage release curve of rifapentine in systems A and B. IBMSCs, Bone marrow mesenchymal stem cells; RPSMs, Rifapentine Poly-lactic Acid Sustained-Release Microspheres. HA/β-TCP, hydroxyapatite/β-tricalcium phosphate.

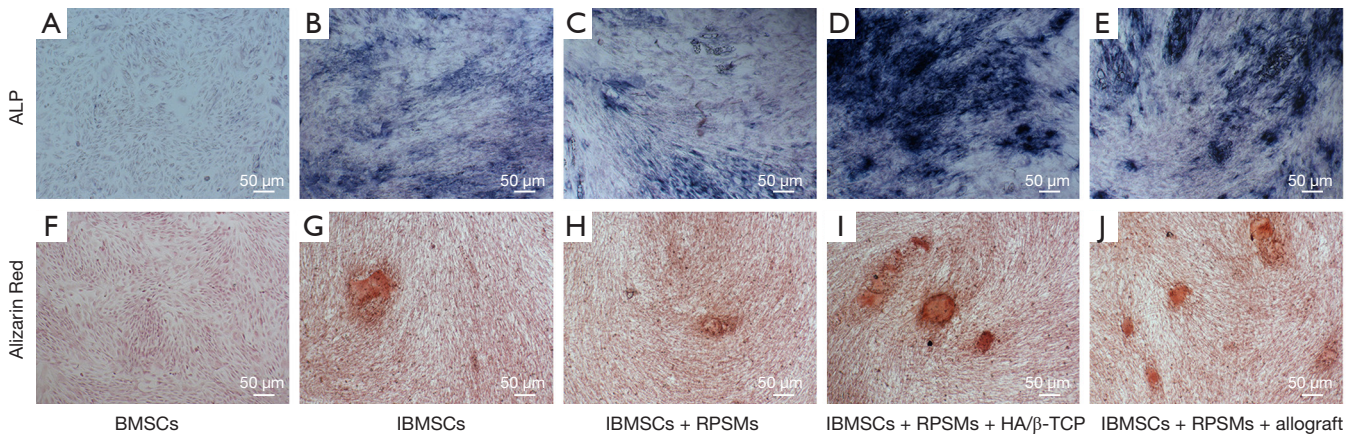


**Figure 7** ALP and Alizarin red staining were used to observe the osteogenic differentiation of the five groups of cells. The ALP (A,B,C,D,E) and Alizarin red (F,G,H,I,J) staining of the five groups of cells were observed under a microscope. (original magnification: 100×, scale bar =50 µm). BMSCs, bone marrow mesenchymal stem cells; IBMSCs, induced bone marrow mesenchymal stem cells; RPSMs, Rifapentine Poly-lactic Acid Sustained-Release Microspheres; ALP, alkaline phosphatase.

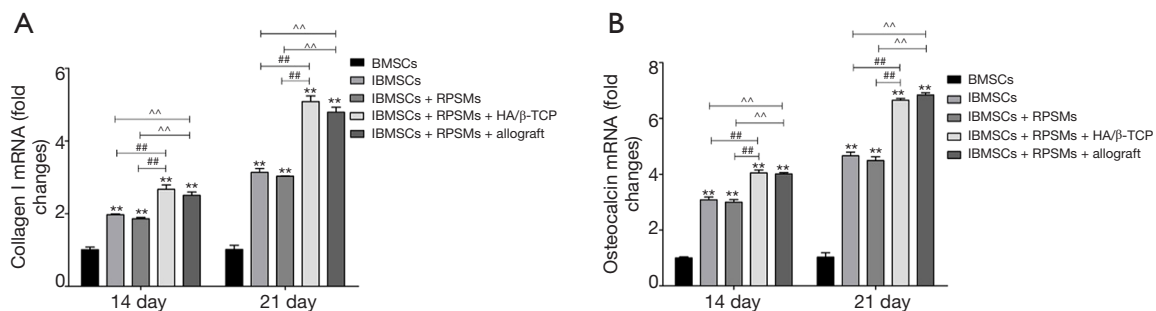


**Figure 8** The mRNA expressions of collagen I and osteocalcin of the five groups of cells were analyzed by quantitative real-time PCR *in vitro*. The expressions of osteogenic marker genes collagen I (A) and osteocalcin (B) were conducted by quantitative real-time PCR. Data were presented as mean ± SD from triplicate samples. \*\*, vs. group A; P<0.01; ##, vs. group D; P<0.01; ^^, vs. group E, P<0.01.

antibiotic drug concentrations and good repair of bone defects at the local site are difficult to achieve through the combination of traditional anti-TB agents with debridement or bone transplantation, and there are a series of side effects (21), making this treatment unsatisfactory for treating patients with osteoarticular TB. Consequentially, we developed sustained drug delivery systems, prepared from BMSCs, RPSMs, and bone graft material, which was placed directly into the lesion site to repair and reconstruct the original bone tissue as well as to treat osteoarticular TB.

The results of our study showed that BMSCs were adherent with a fibroblast-like morphology, expressed the surface markers of BMSC antigens such as CD29 and CD44 (22), and were able to differentiate osteogenically, adipogenically and chondrogenically. These results were consistent with the standards of the International Society for Cell Therapy (23). BMSCs are precursors of osteoblastic-lineage cells, which play a crucial role in bone formation (24). We therefore combined BMSCs with drugs and carriers, constructing sustained drug delivery systems to fill these bone defects and promote bone formation at the lesion.

In recent years, drug delivery systems with sustained release capabilities, such as drug-loaded liposomes and microspheres, have drawn attention. Anti-TB drugs come in the form of tablets and injections, and repeated drug administration can result in significant side effects and poorer patient compliance (25). A sustained-release microsphere, which can deliver a constant, lower drug dose over a long period of time offers a solution to these limitations. For this study, we prepared RPSMs by double emulsion solvent evaporation with PLA and rifapentine. Compared to previous studies, RPSMs had a smooth surface, uniform particle size distribution, and higher encapsulation and drug loading efficiency. This improvement could reduce not only the relative drug release rate but also the administration dosage of microspheres, proving the microspheres were reliably prepared (26). Meanwhile, the antibacterial activity of RPSMs was investigated and *in vitro* results showed that at 8 weeks, RPSMs had better antibacterial activity compared with rifapentine, which indicated that RPSMs have a long-term inhibitory effect on the growth of *Mycobacterium TB*.

To evaluate the possibility of combining BMSCs with anti-TB drugs, the effects of different concentrations of rifapentine on cell proliferation were investigated by CCK-8 assay. Drug concentrations up to 45.0  $\mu\text{g/mL}$

were found to have no effect on cell proliferation, and these concentrations were significantly higher than the minimum inhibitory concentration of rifapentine (0.03–0.06  $\mu\text{g/mL}$ ) (27). Pluripotent stem cell differentiation is closely related to cell cycles, and the regulation of G1 phase is particularly important (28). Cell cycle analysis revealed that the G1 quiescent phase of drug-treated cells was consistent with that of the drug-free cells, with typical stem cell proliferation characteristics and no significant effect on cell differentiation. These results not only made the construction of a sustained drug delivery system possible, but also suggested that the concentration of rifapentine should be kept below 45.0  $\mu\text{g/mL}$ .

In the present study, RPSMs and BMSCs were combined with HA/ $\beta$ -TCP or allogenic bone to form two sustained drug delivery systems. The drug release curve of two sustained drug delivery systems showed a controlled release state, and the drug release peaks were both below 45.0  $\mu\text{g/mL}$ , indicating the microspheres had little effect on cell proliferation during drug release. Furthermore, the sustained drug delivery system formed by HA/ $\beta$ -TCP composite material exhibited a longer duration of drug release. The reason underlying this is that inorganic material can change the polymer degradation behavior by buffering the pH of the nearby solution, thus preventing the hydrolysis of polymer chains, e.g., in PLA (29). Furthermore, the larger pore size of HA/ $\beta$ -TCP composite material promotes the embedding of RPSMs and the adhesion of BMSCs, which obstruct the release of rifapentine from microspheres.

The results of ALP, alizarin red staining, and real-time PCR suggested that RPSMs had no effects on the osteogenic differentiation of stem cells. In addition, the mRNA expression levels of collagen I and osteocalcin were significantly increased in both groups D and E during osteogenic differentiation, with no significant difference between the two groups, which indicated that both materials had good function in relation to osteoinductivity.

Osteoarticular TB always results in massive bone defects that requires bone grafting repair. However, the weak antibacterial ability of bone grafts helps to form a perfect micro-environment for the growth of TB bacteria, and the unrestrained chronic inflammation can lead to a significant reduction in the proliferation capability and differentiation potency of BMSCs, inhibiting bone formation (30). In this study, HA/ $\beta$ -TCP or allogenic bone was combined with RPSMs and BMSCs, respectively, to construct two novel anti-TB drug delivery systems which could not only repair

the bone defects but also inhibit the growth of TB bacteria and reduce the inflammatory response, thus promoting bone formation.

HA/beta-TCP and allogenic bone, which have completely different structures, are commonly used bone graft materials in clinical treatment. Allogenic bone is easily harvested and has similar physical performances with *in situ* bone, which has good osteoconduction and osteoinduction (31). However, the risk of possible related immune reactions and disease transmission also needs to be addressed (32). HA/ $\beta$ -TCP is a common material composed of hydroxyapatite and beta-tricalcium phosphate (33). HA/ $\beta$ -TCP is similar to bone in its molecular composition and structure, and it has excellent biocompatibility and osteoconductive properties (34). Its pore size facilitates cell migration and nutrient/waste exchange (35). Moreover, previous studies have found that HA/ $\beta$ -TCP scaffolds could simulate the 3D microenvironment of bone and promote the osteogenic differentiation of BMSCs (36,37). The results of the drug release test and osteogenic differentiation ability revealed the sustained drug delivery system with HA/ $\beta$ -TCP as scaffold material was more stable and had a longer duration of sustained release, as well as having good biocompatibility, osteoconductivity, and osteoinductivity.

## Conclusions

In this study, we fabricated RPSMs, with an even particle size distribution and ideal anti-bacterium effect, by employing the double emulsion solvent evaporation method, and integrating these microspheres along with BMSCs into HA/ $\beta$ -TCP or allogenic bone to prepare anti-TB drug delivery systems for bone tissue engineering. Further study indicated that the HA/ $\beta$ -TCP-scaffolded drug delivery system was more stable and had a longer duration of sustained release, as well as having good biocompatibility, osteoconductivity, and osteoinductivity. This novel anti-TB drug delivery system for bone tissue engineering can simultaneously serve a purpose in the replacement of bone defects and drug-directed sustained release, and thus provides a new method for the clinical treatment of osteoarticular TB. The therapeutic and tissue repair effects of the drug delivery systems *in vivo* are worthy of further study.

## Acknowledgments

*Funding:* This work was supported by grant 81360283 and

81860394 from the National Natural Science Foundation of China.

## Footnote

*Conflicts of Interest:* The authors have no conflicts of interest to declare.

*Ethical Statement:* The authors are accountable for all aspects of the work in ensuring that questions related to the accuracy or integrity of any part of the work are appropriately investigated and resolved.

*Open Access Statement:* This is an Open Access article distributed in accordance with the Creative Commons Attribution-NonCommercial-NoDerivs 4.0 International License (CC BY-NC-ND 4.0), which permits the non-commercial replication and distribution of the article with the strict proviso that no changes or edits are made and the original work is properly cited (including links to both the formal publication through the relevant DOI and the license). See: <https://creativecommons.org/licenses/by-nc-nd/4.0/>.

## References

1. Gelaw B, Shiferaw Y, Alemayehu M, et al. Comparison of loop-mediated isothermal amplification assay and smear microscopy with culture for the diagnostic accuracy of tuberculosis. *BMC Infect Dis* 2017;17:79.
2. Gu Y, Wu C, Yu F, et al. Application of endobronchial ultrasonography using a guide sheath and electromagnetic navigation bronchoscopy in the diagnosis of atypical bacteriologically-negative pulmonary tuberculosis. *Ann Transl Med* 2019;7:567.
3. Park DW, Chung SJ, Yeo Y, et al. Therapeutic issues with, and long-term outcomes of, pulmonary mycobacterial tuberculosis treatment in patients with autoimmune rheumatic diseases. *J Thorac Dis* 2019;11:4573-82.
4. Muradali D, Gold WL, Vellend H, et al. Multifocal osteoarticular tuberculosis: report of four cases and review of management. *Clin Infect Dis* 1993;17:204-9.
5. Xu Z, Wang X, Shen X, et al. One-stage lumbopelvic fixation in the treatment of lumbosacral junction tuberculosis. *Eur Spine J* 2015;24:1800-5.
6. Yang L, Liu Z. Analysis and therapeutic schedule of the postoperative recurrence of bone tuberculosis. *J Orthop Surg Res* 2013;8:47.

7. Mehnath S, Ayisha Sithika MA, Arjama M, et al. Sericin-chitosan doped maleate gellan gum nanocomposites for effective cell damage in *Mycobacterium tuberculosis*. *Int J Biol Macromol* 2019;122:174-84.
8. Sequeira W, Co H, Block JA. Osteoarticular tuberculosis: current diagnosis and treatment. *Am J Ther* 2000;7:393-8.
9. Ge Z, Wang Z, Wei M. Measurement of the concentration of three antituberculosis drugs in the focus of spinal tuberculosis. *Eur Spine J* 2008;17:1482-7.
10. Wu J, Zuo Y, Hu Y, et al. Development and in vitro characterization of drug delivery system of rifapentine for osteoarticular tuberculosis. *Drug Des Devel Ther* 2015;9:1359-66.
11. Alfarisi O, Alghamdi WA, Al-Shaer MH, et al. Rifampin vs. rifapentine: what is the preferred rifamycin for tuberculosis? *Expert Rev Clin Pharmacol* 2017;10:1027-36.
12. Lasprilla AJ, Martinez GA, Lunelli BH, et al. Poly-lactic acid synthesis for application in biomedical devices - a review. *Biotechnol Adv* 2012;30:321-8.
13. Shive MS, Anderson JM. Biodegradation and biocompatibility of PLA and PLGA microspheres. *Adv Drug Deliv Rev* 1997;28:5-24.
14. Sen MK, Miclau T. Autologous iliac crest bone graft: should it still be the gold standard for treating nonunions? *Injury* 2007;38:S75-80.
15. Dawson J, Kiner D, Gardner W, et al. The reamer-irrigator-aspirator as a device for harvesting bone graft compared with iliac crest bone graft: union rates and complications. *J Orthop Trauma* 2014;28:584-90.
16. Shang F, Ming L, Zhou Z, et al. The effect of licochalcone A on cell-aggregates ECM secretion and osteogenic differentiation during bone formation in metaphyseal defects in ovariectomized rats. *Biomaterials* 2014;35:2789-97.
17. Liu Y, Ming L, Luo H, et al. Integration of a calcined bovine bone and BMSC-sheet 3D scaffold and the promotion of bone regeneration in large defects. *Biomaterials* 2013;34:9998-10006.
18. Kawate K, Yajima H, Ohgushi H, et al. Tissue-engineered approach for the treatment of steroid-induced osteonecrosis of the femoral head: transplantation of autologous mesenchymal stem cells cultured with beta-tricalcium phosphate ceramics and free vascularized fibula. *Artif Organs* 2006;30:960-2.
19. Garg RK, Somvanshi DS. Spinal tuberculosis: a review. *J Spinal Cord Med* 2011;34:440-54.
20. Dunn R, Zondagh I, Candy S. Spinal tuberculosis: magnetic resonance imaging and neurological impairment. *Spine* 2011;36:469-73.
21. Liang Q, Song X, She S, et al. Development of dual delivery antituberculous system containing rifapentine microspheres and adipose stem cells seeded in hydroxyapatite/tricalcium phosphate. *Drug Des Devel Ther* 2019;13:373-84.
22. Sun J, Zhao F, Zhang W, et al. BMSCs and miR-124a ameliorated diabetic nephropathy via inhibiting notch signalling pathway. *J Cell Mol Med* 2018;22:4840-55.
23. Dominici M, Le Blanc K, Mueller I, et al. Minimal criteria for defining multipotent mesenchymal stromal cells. The International Society for Cellular Therapy position statement. *Cytotherapy* 2006;8:315-7.
24. Bianco P, Sacchetti B, Riminucci M. Stem cells in skeletal physiology and endocrine diseases of bone. *Endocr Dev* 2011;21:91-101.
25. Huang J, Chen Z, Li Y, et al. Rifapentine-linezolid-loaded PLGA microspheres for interventional therapy of cavitary pulmonary tuberculosis: preparation and in vitro characterization. *Drug Des Devel Ther* 2017;11:585-92.
26. Klose D, Siepmann F, Elkharraz K, et al. How porosity and size affect the drug release mechanisms from PLGA-based microparticles. *Int J Pharm* 2006;314:198-206.
27. Rastogi N, Goh KS, Berchel M, et al. Activity of rifapentine and its metabolite 25-O-desacetyl-rifapentine compared with rifampicin and rifabutin against *Mycobacterium tuberculosis*, *Mycobacterium africanum*, *Mycobacterium bovis* and *M. bovis BCG*. *J Antimicrob Chemother* 2000;46:565-70.
28. Dalton S. Linking the Cell Cycle to Cell Fate Decisions. *Trends Cell Biol* 2015;25:592-600.
29. Mouriño V, Boccaccini AR. Bone tissue engineering therapeutics: controlled drug delivery in three-dimensional scaffolds. *J R Soc Interface* 2010;7:209-27.
30. Bastian OW, Croes M, Alblas J, et al. Neutrophils Inhibit Synthesis of Mineralized Extracellular Matrix by Human Bone Marrow-Derived Stromal Cells In Vitro. *Front Immunol* 2018;9:945.
31. Kim YK, Lee JY, Kim SG, et al. Guided bone regeneration using demineralized allogenic bone matrix with calcium sulfate: case series. *J Adv Prosthodont* 2013;5:167-71.
32. Ferracini R, Martínez Herreros I, Russo A, et al.

- Scaffolds as Structural Tools for Bone-Targeted Drug Delivery. *Pharmaceutics* 2018;10:122.
33. Bellucci D, Sola A, Cannillo V. Hydroxyapatite and tricalcium phosphate composites with bioactive glass as second phase: State of the art and current applications. *J Biomed Mater Res A* 2016;104:1030-56.
  34. Gamie Z, Tran GT, Vyzas G, et al. Stem cells combined with bone graft substitutes in skeletal tissue engineering. *Expert Opin Biol Ther* 2012;12:713-29.
  35. Gupta A, Kukkar N, Sharif K, et al. Bone graft substitutes for spine fusion: A brief review. *World J Orthop* 2015;6:449-56.
  36. Bassi G, Guilloton F, Menard C, et al. Effects of a ceramic biomaterial on immune modulatory properties and differentiation potential of human mesenchymal stromal cells of different origin. *Tissue Eng Part A* 2015;21:767-81.
  37. Mebarki M, Coquelin L, Layrolle P, et al. Enhanced human bone marrow mesenchymal stromal cell adhesion on scaffolds promotes cell survival and bone formation. *Acta Biomater* 2017;59:94-107.

**Cite this article as:** Wang Z, Song X, Yang H, Maimaitiaili A, Wang T. Development and *in vitro* characterization of rifapentine microsphere-loaded bone implants: a sustained drug delivery system. *Ann Palliat Med* 2020;9(2):375-387. doi: 10.21037/apm.2020.03.13